Residual stresses in DLC/Si and Au/Si systems: Application of a stress-relaxation model to the nanoindentation technique

Yun-Hee Lee and Dongil Kwon[a]
School of Materials Science and Engineering, Seoul National University, Seoul 151-742, Korea

(Received 5 July 2001; accepted 31 January 2002)

Residual stress in a thin film was analyzed by the nanoindentation technique. Two dominant effects of residual stress to indentation were summarized as the slope change in loading curve and the invariant value of intrinsic hardness. A stress-sensitive reversibly deformed zone around contact was modeled to explain the indentation behaviors under a residually stressed state. Finally, the residual stress was evaluated from the changes in contact shape and applied load during stress relaxation under the condition of constant indentation depth. The residual stresses in diamond-like carbon and Au films analyzed from this model agreed well with the average values measured by the curvature method.

I. INTRODUCTION

Residual stress generated by local plastic deformation or inhomogeneous heat treatment reduces the fatigue strength and fracture properties of bulk materials.[1] In the case of thin films, the residual stress dominates the mechanical properties.[2–5] However, current stress-measuring techniques[1,6–8] have some problems with stress relaxation during specimen sampling, removal of the local material without damage,[6] and complex and time-consuming testing procedures.[1,6,7] The conventional curvature method using a laser beam[7,9] often employed to measure residual stress in thin films cannot be used for a rough film surface and cannot identify local variations in residual stress.

Nanoindentation was proposed as an *in situ* and nanometer-order local stress-analysis technique. In particular, the nanoindentation technique has significance because it has been widely applied in characterizing the basic mechanical properties of thin films.[10,11] The results of previous studies on residual stress using macroindentation were empirical measurements of the variations in the apparent hardness[12] or the shape of the residual indentation mark.[13] Another study[14] attempted to determine a relationship between the apparent hardness from the analysis of the load–depth curve and the residual stress. However, recent accurate observation[15] of the indentation mark and indentation simulation[16] using the finite element analysis verified the independence of the residual stress and the intrinsic hardness. Furthermore, a theoretical analysis[17] was already made of the effect of stress on the shape variation of the indentation curve. However, the distinct stress effects on indentation curve and contact morphology were not proposed in the analysis. Thus, more fundamental studies on the residual stress effect to nanoindentation are still required.

Therefore, the thin-film residual stress was evaluated quantitatively by a theoretical analysis of the stress-influential nanoindentation factors. The changes in the contact morphologies were modeled on the basis of the assumption of an invariant intrinsic hardness regardless of the residual stress beneath a sharp indenter. The morphology change around the contact was analyzed as a stress-induced factor from the indentation loading curve during stress relaxation. The residual stress in a thin film was calculated from the residual stress-induced factor. The evaluated value was consistent with the result from the conventional curvature method and showed the potential of the indentation method as a stress-probing technique.

II. THEORETICAL ANALYSIS

A. Interaction between residual stress and indentation load

The residual stress in a thin film is assumed as an in-plane isotropic state. In addition, the stress gradient in the thickness direction is negligible for a shallow indentation (less than one-tenth of the film thickness). The change in indentation deformation caused by the residual stress was identified in the indentation loading curve shown in Fig. 1. The applied load of the tensilely stressed thin film is lower than that of a stress-free film for the same maximum indentation depth.[15–17] In other words, the maximum indentation depth desired is reached at a smaller indentation load in a tensilely stressed film, because a residual-stress-induced normal load acts as an additive load to the applied load. Unlike the case for the tensilely stressed state, the applied indentation load of a compressively stressed thin film increases in an equal

[a]Address all correspondence to this author.
e-mail: donglik@gong.snu.ac.kr

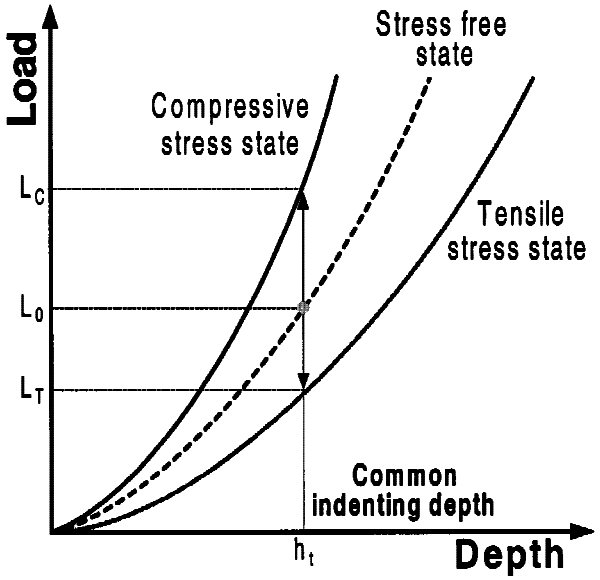

FIG. 1. Variation of the indentation loading curves with the changes in the stress states.[15,17]

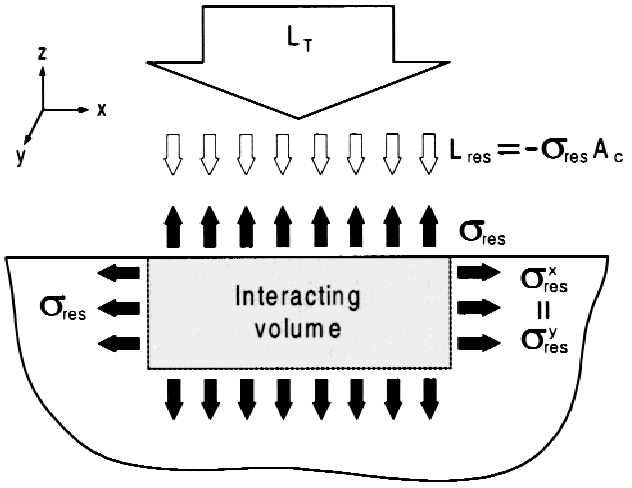

FIG. 2. Interaction of the residual-stress-induced normal load, L_{res}, and the indentation load, L_T.

quantity of the residual-stress-induced normal load. Therefore, the residual stress in a thin film can be evaluated by analyzing the residual-stress-induced normal load.

The direction and quantity of the residual-stress-induced normal load were discussed in a recent report.[17] Hardness, i.e., the extent of plastic deformation, was independent of the hydrostatic stress state. Therefore, the biaxial in-plane stress in a thin film was treated as equivalent to uniaxial stress subtracted from the triaxial stress. In other words, the biaxial tensile residual stress ($\sigma^x_{res} = \sigma^y_{res}$) can be found by adding uniaxial compressive stress to the triaxial tensile stress as shown in the schematic diagram in Fig. 2. The effect of the residual stress on an applied load, L_T, is expressed as the residual-stress-induced normal load, L_{res}. Furthermore, this additive load is a multiple of the contact area and σ_z:

$$\sigma^x_{res} = \sigma^y_{res} = \sigma_{res} \quad , \qquad \sigma_z = -\sigma_{res} \quad . \tag{1}$$

Several studies[15–17] have reported that the intrinsic hardness and the contact area between the indenter and specimen were not altered by the effect of residual stress, which is contrary to variations in the indentation load–depth curve. Therefore, the contact morphology was modeled to satisfy the invariant intrinsic hardness and the variation in the indentation loading curve by the action of L_{res}.

B. Change in contact morphology with residual stress

The exact measurement of the contact area is indispensable for evaluating the hardness, because the hardness, which represents the degree of plastic deformation, is obtained by dividing the indentation load by the contact area. The measured hardness is affected by various measurement errors arising from surface roughness or optical observation and thus referred to as the apparent hardness. In addition, this apparent hardness was used as a parameter of the residual stress in initial studies.[12,14] However, the variations in the apparent hardness with a change in the residual stress have also been identified as artifacts of erroneous optical measurements of the indentation mark. Recently, the intrinsic hardness has been reported as invariant regardless of the residual stress in studies using finite element analysis[16] and fine observations of the indentation mark[15] by scanning electron or atomic force microscopes. Therefore, the change in contact morphologies with residual stress was modeled for constant maximum indentation depth, with the results shown in Fig. 3, assuming the independence of the intrinsic hardness and the residual stress. The applied load increases from L_T to L_C through L_0 with changes in the residual stress from (a) tensile through (b) stress-free to (c) compressive states for a given indentation depth. In addition, the contact area increases with increasing applied load for the invariant value of the intrinsic hardness:

$$H = L_T/A^T_c = L_0/A_c = L_C/A^C_c \quad . \tag{2}$$

This variation in the contact depth due to the residual stress for a given indentation depth converges reversibly to the contact depth for the stress-free state shown in Fig. 3(b) by the stress-relaxation procedure. Thus, the effect of residual stress on indentation is explained as the elastic deformation around the contact. The large/small contact depths in the tensile/compressive stress states were modeled with the aid of the elastic pile-up depth (h_p)/sink-in depth (h_n) as shown in Figs. 3(a) and 3(c), respectively.

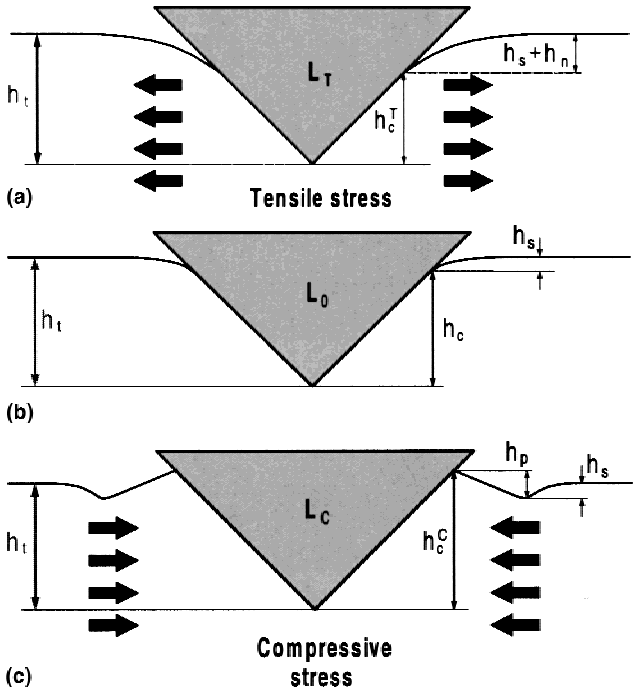

FIG. 3. Theoretical surface morphologies around the contact for (a) tensile stress, (b) stress-free, and (c) compressive stress states.

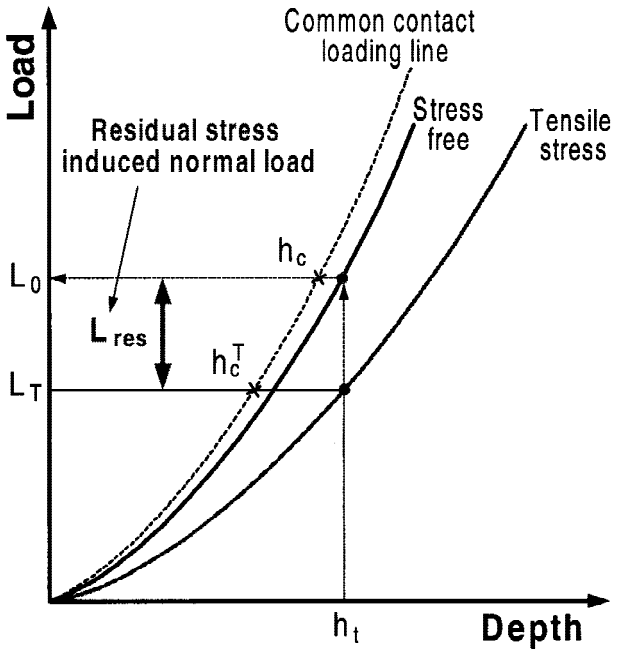

FIG. 4. Change in the applied indentation load during stress relaxation by the maximum-depth-controlled path.

C. Modeling of indentation-depth-controlled stress relaxation

The loading curve from nanoindentation has a lower slope in the tensilely stressed state than the stress-free state, as shown in Fig. 1, and a higher slope in the compressively stressed state. The applied load increases from L_T to L_C through L_0 with changing stress state from tension to compression through the stress-free point for a constant maximum indentation depth, h_t. A stress-relaxation procedure controlling the maximum depth as a constant is shown in Fig. 4. One common contact depth corresponds to an indentation load that satisfies the residual-stress-independent intrinsic hardness. The common contact loading line was made by connecting each calculated common contact depth for each indentation load. The applied load, L_0, at the stress-free state increases by stress relaxation from the load, L_T, in the tensile stress state for a given maximum depth, h_t. The differential load, $L_0 - L_T$, is the residual stress-induced normal load, L_{res}. In addition, the detailed changes in contact morphology can be explained from the schematic diagram shown in Figs. 3(a) and 3(b). The residual stress is relaxed for a tensilely stressed specimen maintaining the constant maximum depth, h_t, as the stress relaxation pushes the indenter out from the surface. However, the pushing force appears as the increase in the applied load ($L_T \rightarrow L_0$) and the contact depth ($h_c^T \rightarrow h_c$), because the maximum depth is held constant. The indentation load and maximum depth for the tensilely stressed state (L_T, h_t) is equivalent to those in the relaxed state (L_0, h_t). Thus, the relationship between the two states can be expressed as

$$L_0 = L_T + L_{res} \quad . \tag{3}$$

In the compressive stress state, the applied load and contact depth decrease by stress relaxation under the maximum-depth-controlled path. Furthermore, this decreasing portion of the applied load was the residual-stress-induced normal load, L_{res}. Therefore, the residual stress in a thin film can be evaluated by dividing L_{res} by the contact area, A_c, regardless of the stress state:

$$\sigma_{res} = L_{res}/A_c \quad . \tag{4}$$

III. EXPERIMENTAL PROCEDURES

The nanoindentation test used to evaluate the residual stress in thin films through the stress-relaxation model was performed as follows. First, diamond-like carbon (DLC) and Au thin films were deposited on Si wafers using chemical vapor deposition and E-beam evaporation, respectively. The thickness of the DLC film was 0.6 μm, and that of the Au film was 1.0 μm. A stress-free film was needed for comparison with the residually stressed film. Thus, a free-standing film was formed by removing the Si substrate. Nearly all the residual thermal and intrinsic stresses in the thin films, except for the small stress resulting from growth defects, were removed by removal of the substrate. For the DLC/Si system, Si was

dissolved in a 60% HNO_3 + 30% HF + 10% CH_3COOH solution by a wet-etching technique, thereby removing the substrate. In the case of the Au film, the interfacial adhesion was so poor that the Au thin film was physically peeled from the Si substrate without damage. The free-standing films were rinsed with ethyl alcohol, placed on a Si base without adhesive, and indented. The maximum indentation depth was determined to be less than one-tenth of the film thickness, thus excluding the effect of substrate deformation.[18] The indentation loads satisfying the condition of maximum indentation depths were 2000 μN for DLC and 1500 μN for Au films. Nanoindentation was done with a loading speed of 250 μN/s using a Berkovich indenter.

The average value of the surface residual stress was measured using the conventional curvature method. The scan length of the laser source on the film surface was 20 mm. The average residual stress was analyzed from the measured curvature radius of thin film using Eq. (5):

$$\sigma_{res} = Et^2/6(1-\nu^2)t_f R \quad , \qquad (5)$$

where E, t, and ν are the elastic modulus, thickness, and Poisson ratio of the substrate, respectively, and t_f and R are the film thickness and curvature radius.

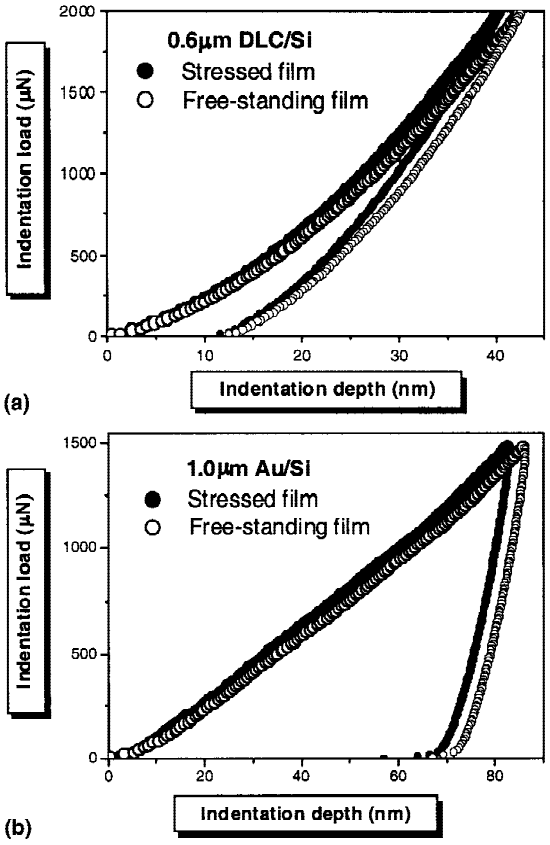

FIG. 5. Shape change in indentation load–depth curves for (a) DLC/Si and (b) Au/Si from the effect of the thin-film residual stress.

IV. RESULTS AND DISCUSSION

The shape change in the indentation curve induced by stress relaxation is displayed in Fig. 5 for DLC and Au thin films. The load–depth curves from the as-deposited film were reproducible, unlike those from the free-standing films. For the free-standing film, the slope of initial loading part was very low, due to the compression of the air gap between the free-standing film and the Si base during indentation (no adhesive was used, to avoid the formation of additive residual stress from interfacial bonding). The slope of the loading curve increased after tight attachment of the film to the base. Therefore, the leftmost curve without the air gap effect was selected from the 10 testing curves of the free-standing film. All analyzed curves shown in Fig. 5 displayed the representative deformation behavior of all as-deposited and free-standing films. The loading curves for the as-deposited DLC and Au films were located to the left of the loading curves for the free-standing films, thus confirming that the residual stresses in the two films were compressive.

The assumption of invariant intrinsic hardness was confirmed by direct observation of an indentation mark using atomic force microscopy (AFM). The apparent hardnesses of the DLC film from conventional curve analysis were 23.4 GPa for the as-deposited and 21.1 GPa for the free-standing films. The apparent hardness of the as-deposited film was overestimated more than 10.9% compared to that of the free-standing film. However, the effect of residual stress on the real contact length from the cross-sectional AFM image shown in Fig. 6 was negligible: the difference in the contact length between

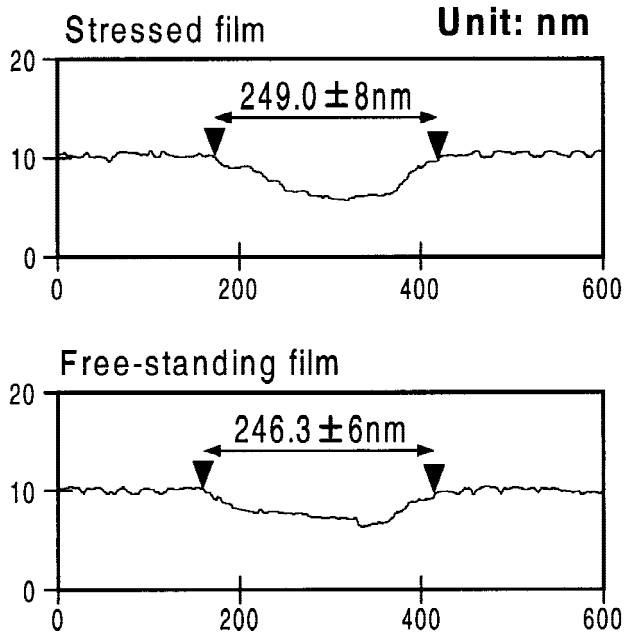

FIG. 6. Invariant contact lengths in DLC film regardless of the stress state.

the stressed and stress-free states was only 1.1%. The contact lengths were 249.0 ± 8 nm for the as-deposited and 246.3 ± 6 nm for the free-standing films. The assumption of stress-independent intrinsic hardness was verified from this result. However, an exact measurement of the contact length in the Au film was impossible due to the complex shape of plastic pile-up.

The contact area for the stress-free state, A_c, and the residual-stress-induced normal load, L_{res}, were analyzed to evaluate the thin film residual stress from the shape change in the indentation loading curve in Fig. 5. L_{res} was measured as the difference in the indentation load from the effect of residual stress at a given indentation depth. The contact area, A_c, corresponding to the contact depth, h_c, on the common contact loading line at a given indentation depth was evaluated by analyzing the indentation unloading curve on the basis of the invariant elastic modulus of thin film regardless of the indenter penetrating depth. The elastic modulus was evaluated from the indentation curve for the stress-free film using the flat punch theory.[10] The indentation unloading curve was fitted as a power law. The initial stiffness, S, and the contact depth, h_c, were determined from the tangent to the power-fitted curve as the initial slope and the intercept depth, respectively. Then, the contact area, A_c, was determined using the tip-area function in Eq. (6). (The actual shape of the pointed Berkovich indenter was calibrated by assuming a constant elastic modulus regardless of the increase of indentation depth in a standard material such as fused quartz.)

$$A_c = C_0 h_c^{\,2} + C_1 h_c + C_2 h_c^{\,1/2} + C_3 h_c^{\,1/4} + C_4 h_c^{\,1/8} + C_5 h_c^{\,1/16} \quad , \tag{6}$$

where C_0 is a constant of 24.5, from the ideal geometry of the Berkovich indenter. The values of C_1 to C_5 were empirically determined by the polynomial-fitting procedure. In addition, the stiffness was expressed in terms of the contact depth as shown in Eq. (7):

$$S = L_{max}/(h_{max} - h_c) \quad . \tag{7}$$

The reduced elastic modulus, E_r, including the elastic properties of a thin film and indenter, was expressed using the terms S and A_c as shown in Eq. (8):[10,11]

$$E_r = \pi^{1/2} S/(2A_c^{\,1/2}) = \pi^{1/2} L_{max}/[2A_c^{\,1/2}(h_{max} - h_c)] \quad . \tag{8}$$

Thus, the contact depth and area for each analyzed load can be evaluated from Eqs. (6) and (8) by inputting the constant value of E_r. The reduced elastic moduli of the DLC and Au free-standing films were 493.2 and 142.2 GPa, respectively. The elastic modulus and the Poisson's ratio of the diamond indenter are 1141 GPa and 0.07, respectively.[15]

Finally, the residual stresses in the thin films were evaluated by inputting the measured residual-stress-induced normal load and the analyzed contact area into Eq. (4) for various indentation load steps as shown in Fig. 7 and Tables I and II. The evaluated residual stress decreased with increasing indentation load and contact depth. The corresponding stress values for the surface residual stress from the conventional curvature method were obtained from the shallow indentation region (less than 5% of the film thickness). The analyzed residual stresses from nanoindentation were −3.75 GPa and −104.8 MPa for the DLC and Au films in this shallow contact depth region, respectively. These values were consistent with the residual stresses of −3.8 ± 0.5 GPa and −93.4 ± 28.5 MPa obtained from the curvature method.

The decrease in residual stress with increasing indentation depth can be explained in two ways. First, a stress gradient can affect nanoindentation: the bending residual stress in the thin film decreases with increasing penetration depth from the surface to the interior. Therefore, with increasing contact depth, the indenter probes lower residual stresses than at the surface. The other explanation appeals to the enlarged plastic deformation region around the indenter. The stress-relaxation behavior was

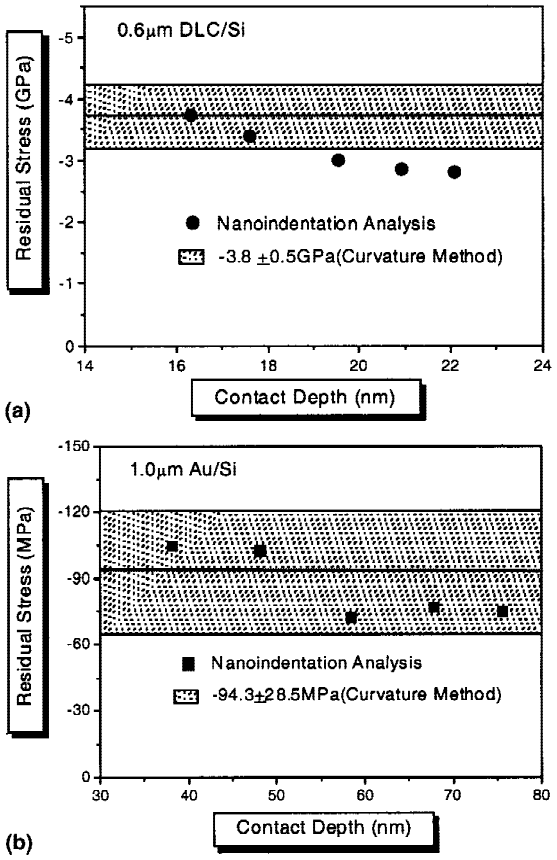

FIG. 7. Comparisons of the analyzed residual stress values for (a) DLC/Si and (b) AU/Si with results from the curvature method.

TABLE I. Residual stress values for the DLC film analyzed at various contact depths.

Indentation load (μN)	Stress-induced load (μN)	Contact area (nm^2)	Residual stress (GPa)
1950	158.3	56059.5	−2.82
1850	147.3	51238.9	−2.88
1750	138.2	45720.4	−3.02
1650	132.0	38546.3	−3.42
1550	128.2	34227.6	−3.75

TABLE II. Residual stress values of the Au film analyzed at various contact depths.

Indentation load (μN)	Stress-induced load (μN)	Contact area (nm^2)	Residual stress (MPa)
1450	79.47	1062624.7	−74.8
1250	70.56	915775.6	−77.1
1050	53.98	749486.1	−72.2
850	60.00	585475.8	−102.5
650	49.22	469661.2	−104.8

modeled at the elastic deformation around the contact. However, the plastically deformed region beneath the indenter can expand beyond the contact area at a higher indentation load. In addition, the sensitivity of indenter to the residual stress decreases with increasing distance between the indenter and the stress-sensitive elastically deformed zone around the plastic zone. Therefore, error in the evaluated residual stress increases with increasing indentation loads and depth.

V. CONCLUSIONS

The residual stresses in the DLC and Au films were evaluated by analyzing the stress-induced shape change in the indentation loading curve and the contact morphology during stress relaxation. The validity of the relaxation model was confirmed by the agreement of the stress value with the results from the curvature method. The major conclusions of this study are as follows:

(1) The intrinsic hardness and contact area from AFM observations were invariant for DLC films regardless of the residual stress, which agrees with the assumption of our relaxation model. The decrease in contact length was only 1.1% during stress relaxation from the high compressive stress state of −3.8 GPa in DLC film.

(2) A region sensitive to elastic residual stress was modeled as the reversible deformation zone around the contact area. The contact morphology agreed with the two significant effects of residual stress, namely the shape change in the loading curve and the invariant contact depth for a given applied load.

(3) An equation for the residual stress was proposed from the analysis of the additive stress-induced normal load and the change in contact morphology during stress relaxation under maximum depth control.

(4) The effects of compressive residual stresses in the DLC and Au films were identified from the indentation results for the free-standing and the as-deposited films under the same conditions. The residual stresses were analyzed for various indentation load steps using the theoretical modeling proposed in this study. The values calculated for the DLC and Au films were −3.75 GPa and −104.8 MPa, respectively. These correspond well with the −3.8 GPa and −93.4 MPa calculated from the curvature method for the two respective thin films.

REFERENCES

1. I.C. Noyan and J.B. Cohen, *Residual Stresses* (Springer-Verlag, New York, 1987).
2. A.W. Eberhardt, R. Pandey, J.M. Williams, J.J. Weimer, D. Ila, and R.L. Zimmerman, Mater. Sci. Eng. A **229,** 147 (1997).
3. L. Karlsson, L. Hultman, and J.E. Sundgren, Thin Solid Films **371,** 167 (2000).
4. E. Uhlmann and K. Klein, Surf. Coat. Technol. **131,** 448 (2000).
5. W. Fang and C-Y. Lo, Sens. Actuators **84,** 310 (2000).
6. C.O. Ruud, P.S. DiMascio, and J.J. Yavelak, Exp. Mech. **25,** 338 (1985).
7. A.J. Perry, J.A. Sue, and P.J. Martin, Surf. Coat. Technol. **81,** 17 (1996).
8. L. Bergman and R.J. Nemanich, J. Appl. Phys. **78,** 6709 (1995).
9. P.A. Flinn, in *Thin Films: Stresses and Mechanical Properties Proc. 130,* edited by J.C. Brauman, W.D. Nix, D.M. Barnett, and D.A. Smith (Mater. Res. Soc. Symp. Proc. **130,** Pittsburgh, PA, 1989), p. 41.
10. M.F. Doerner and W.D. Nix, J. Mater. Res. **1,** 601 (1986).
11. G.M. Pharr and W.C. Oliver, MRS Bull. July, 28 (1992).
12. G. Sines and R. Carlson, ASTM Bull. February, 35 (1952).
13. J.H. Underwood, Exp. Mech. **13,** 373 (1973).
14. W.R. LaFontaine, C.A. Paszkiet, M.A. Korhonen, and C-Y. Li, J. Mater. Res. **6,** 2084 (1991).
15. T.Y. Tsui, W.C. Oliver, and G.M. Pharr, J. Mater. Res. **11,** 752 (1996).
16. A. Bolshakov, W.C. Oliver, and G.M. Pharr, J. Mater. Res. **11,** 760 (1996).
17. S. Suresh and A.E. Giannakopoulos, Acta Mater. **46,** 5755 (1998).
18. T.Y. Tsui and G.M. Pharr, J. Mater. Res. **14,** 292 (1999).